ORIGINAL RESEARCH ARTICLE

# Measuring Dynamic Nonreactive Wetting Behavior Between Interstitial-Free Molten Steel and Alumina

QIAN LONG, WANLIN WANG, and XU GAO

An improved sessile drop method was used to measure the dynamic nonreactive wetting behavior of different titanium concentrations interstitial-free molten steel on an alumina substrate at 1550 ºC, and the interfacial tension was also calculated by Young' equation based on the measured surface tension and the static contact angle compared to the previous sessile drop method. And the discrepancies were investigated by analyzing the interface layer between the melt and the alumina substrate with different oxygen partial pressures. Furthermore, it was discussed for the forces analysis of the dynamic contact angle for the improved sessile drop method and the interface layer reactive for the improved sessile drop method. The results demonstrate that the advancing angle, receding and static contact angles between the flowing melt and the solid substrate were quickly obtained by the improved sessile drop method. And the interfacial tension between molten steel and alumina substrate, which is 1428.71 and 1221.35 mN/m, respectively, with titanium concentrations of 280 ppm and 540 ppm for the improved sessile drop method, is higher than for the previous sessile drop method, which is 1245.56 and 719.01 mN/m, respectively. The low alloy interstitial-free molten steel and alumina substrate had formed an interface layer for the previous sessile drop method, and the thickness of the interface layer increased from 3.5 to 77.8 $\mu$m with a titanium concentration of 540 ppm as the oxygen partial pressure increased from $5.4 \times 10^{-23}$ to $5.4 \times 10^{-19}$ atm. The interface layer, which is composed of alloy compounds such as silicon, manganese and titanium oxides, is sensitive to the active alloy of interstitial-free molten steel and oxygen partial pressure.

https://doi.org/10.1007/s11663-024-03065-7


## I. INTRODUCTION

Interfacial wettability is usually characterized by contact angle, which is directly related to surface tension and interfacial tension. The surface tension of a liquid is an essential physical parameter, which is due to the liquid's tendency to lower its surface area. At the boundary between liquid and gas, an extremely small pulling force is generated due to the attraction between the molecules. This pulling force of the liquid is called surface tension. Furthermore, at the boundary between liquid and either liquid or solid, which do not dissolve each other, an extremely small pulling force is generated at the interface. This is called the interfacial tension between the liquid phase and either the liquid or solid phase.[1]

The interfacial wetting behavior of an alloy containing molten steel and an alumina ceramic matrix has a significant impact on iron and steel making.[2–4] Generally, the wetting characteristics between the ceramic-based refractory material and the low alloy steel could affect the life of the refractory, and the wetting characteristics between the refractory and the low alloy steel could affect the interface reaction, thereby reducing the purity of the steel liquid. And the interfacial tension between molten steel and alumina inclusions is very important to the behavior and removal of inclusions in molten steel.[5,6] Furthermore, the dynamic wetting behavior could also be formed between the liquid steel and the solid copper/ceramics mold due to the gravity and flow of the liquid steel. Generally, the shear force parallel to the solid mold could lead to the formation of the advancing contact angle during the early stage of the casting process, as shown in Figure 1(a), and the gravity parallel to the solid mold could lead to the formation of the receding contact angle during the tail stage of pourings, as shown in Figure 1(b). Obviously, there is a dynamic wetting behavior between the contained alloy molten steel and the solid casting mold, which is an important parameter regarding metal solidification, billet quality and heat transfer between the solid and steel liquid.[7,8]

QIAN LONG, WANLIN WANG, and XU GAO are with the School of Metallurgy and Environment, Central South University, Changsha, 410083 P.R. China and also with the National Center for International Research of Clean Metallurgy, Central South University, Changsha, 410083 P.R. China. Contact e-mail: wanlin.wang@gmail.com; xgao.sme@csu.edu.cn
Manuscript submitted May 6, 2023; accepted March 4, 2024.
Article published online March 27, 2024.

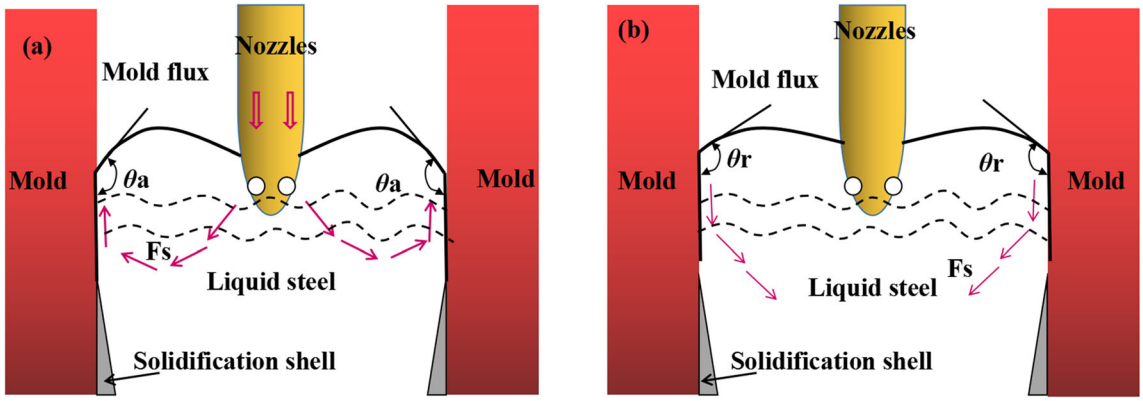


Fig. 1—Typical wetting behavior between molten steel and the casting solid mold during (*a*) the early stage of the casting process and (*b*) the tail stage of pouring.

The measurement method of liquid surface tension was divided into the statics method and the kinetic method. Static methods included the capillary ascending method, the du Noüy ring method, the Wilhelmy disk method, the spinning drop method, the hanging drop method, the sessile drop method and the maximum bubble pressure method; dynamic method included the oscillating jet method and the capillary wave method. At present, for high-temperature melting, the sessile drop method is commonly used to measure surface tension using the Laplace formula.[9,11–18] What is more, the interfacial tension between liquid and solid was calculated by Young's equation.[12]

However, the contained alloy molten steel is especially sensitive to the surrounding environmental oxidative atmosphere at high temperature.[19,20] Generally, the protective gas argon could be purified with reducing metal shavings such as Mg, Cu and Ti, perhaps a certain amount of reducing gas such as $H_2$ or CO could be introduced during the experiment.[12] And, it is difficult to avoid the interface reaction between the contained alloy molten steel and the substrate that forms reactive-wetting behavior due to the long-term mutual contact, which could influence the accuracy of the measurement.[21] On the other hand, the contained active alloy molten steel could react with solid substrate materials, which could also influence the accuracy of the measurement.[22,23]

In this paper, compared with the previous sessile drop method, an improved sessile drop method that could obtain the dynamic contact angle was used to measure the surface tension of interstitial-free molten steel, and interfacial tension was calculated by Young's equation based on the measured surface tension and contact angle between interstitial-free molten steel and an alumina substrate at temperatures 1550 °C under oxygen partial pressure $5.4 \times 10^{-23}$ atm. And the mechanism leading to this difference between the two methods was clarified by investigating the interface reactive layer for different titanium concentrations under oxygen partial pressure $5.4 \times 10^{-23}$ and $5.4 \times 10^{-19}$ atm. Furthermore, the forces analysis of the dynamic contact angle for the improved sessile drop method and the reaction behavior of the interfacial layer for the previous sessile drop method were discussed.

## II. APPARATUS AND METHOD

The improved sessile drop and previous sessile drop techniques were used in the present study to measure the surface tension of interstitial-free molten steel and contact angles between molten steel and solid alumina substrates at temperatures 1550 °C. And, the interfacial tension between molten steel and alumina substrates was calculated by Young' equation based on both the surface tension and the measured statics contact angles.

### A. *Materials Preparation*

In order to reveal the effect of alloy elements in molten steel on the two method, the samples of interstitial-free steel were prepared using high-frequency induction melting under an inert argon gas protective atmosphere (Ar > 99.999 pct). The titanium alloys were added to the actual production melt steel to adjust the composition of the interstitial-free steel. The sample composition after ultrasonic cleaning was analyzed as shown in Table I. Samples A and B have different alloy titanium concentrations of 280 and 540 ppm, respectively. And there are trace amounts of active Si, Mn and Al in the samples of interstitial-free steel. Additionally, a prepared polycrystalline alumina substrate of 40*60*5 $mm^3$ was polished smoothly, and the average roughness was less than 5.6 $\mu$m with a confocal laser scanning microscope (CLSM) after analyzing the surface three-dimensional morphology, as shown in Figure 2.

### B. *Apparatus and Procedure*

The improved sessile drop method and previous sessile drop method, as shown in Figures 3 and 4 were used to measure the surface tension of interstitial-free molten stee and contact angles between the molten steel and the alumina substrates. For improved sessile drop method as shown Figure 3, it was main consisted of four part including controlling protective atmosphere, high-frequency induction melting, Infrared thermometer and Image acquisition system. An 8*12 mm cleaned cylinder sample (constant mass 8 ± 0.01 g) was taken into a quartz tube with an inner diameter of 10 mm and

Table I. Main Alloy Chemical Composition of Steel Samples (Wt Pct)

| | Ca | Ti | Al | Si | Mn | S | P | C | O | N | Fe |
|---|---|---|---|---|---|---|---|---|---|---|---|
| A | 0.0006 | 0.0280 | 0.0170 | 0.0017 | 0.0821 | 0.0033 | 0.0149 | 0.0017 | 0.0019 | 0.0016 | bal. |
| B | 0.0006 | 0.0540 | 0.0170 | 0.0017 | 0.0821 | 0.0033 | 0.0149 | 0.0017 | 0.0020 | 0.0016 | bal. |

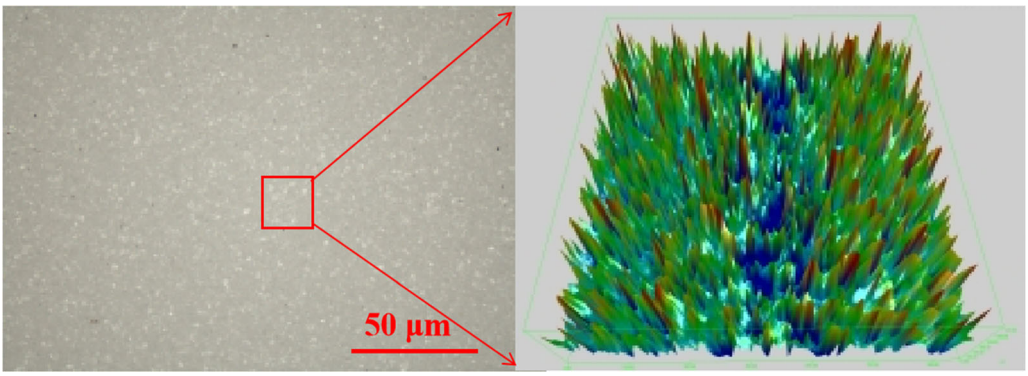


Fig. 2—Polycrystalline alumina substrate and the morphology of surface.

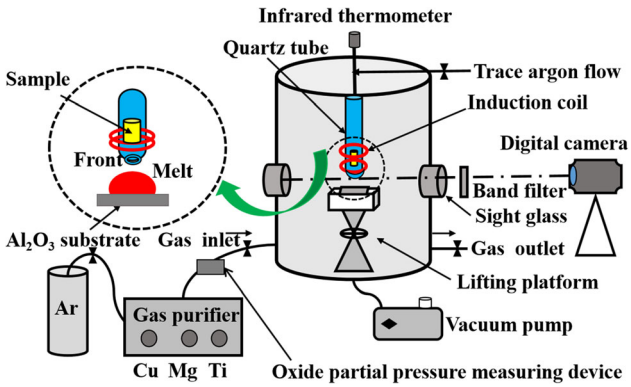


Fig. 3—Schematic diagram of the improved sessile drop method structure.

a front diameter of 1.5 mm, adjusting the height between the front of the quartz tube and the alumina substrate (H) to about 15 mm via a lifting platform. The furnace body evacuating for three times with a vacuum pump and protecting under high-purity argon gas purified with copper, magnesium and titanium metals at 400 ºC. The sample was melted under high-purity argon gas with a high-frequency induction coil, which was cooled by flowing water. The molten steel sample at 1550 ºC measured by an infrared thermometer, dropped down along the front of a quartz tube by trace argon flow and stayed steadily on the alumina substrate, which was recorded by a digital camera named the JVC-GC-P100 HD memory camcorder through the band filter and sight glass. Then the contact angle was obtained by by a general-purpose image analysis program for Image-J with the specialized plugin LB-ADSA. It is noticed that the temperature of the alumina substrate may also affect the interface characteristics measured between the steel liquid and the alumina. Therefore, the temperature before the steel liquid drops is kept consistent, and the interface characteristics are measured before the steel liquid re-shines to avoid the influence of the alumina substrate temperature on the measurement as much as possible.

For the previous sessile drop method, as shown in Figure 4, the experimental procedures were reported in related literature.[11–18] Here, an 8*12 mm cleaned cylinder sample placed on alumina substrate was melted at 1550 ºC under protective argon gas, which was purified with copper, magnesium and titanium metals at 400 ºC for oxide partial pressure of $10^{-23}$ atm. It's worth noting that the values of oxide partial pressure measured in the experiment were about $10^{-18}$ to $10^{-23}$ atm. The partial pressure of oxygen in the furnace could be controlled by a valve at the gas inlet.

## III. DETAILED METHODOLOGY

On the one hand, the interfacial properties between alumina and samples A and B were determined by the improved sessile drop method and the previous sessile drop method under an oxygen partial pressure $5.4 \times 10^{-23}$ atm. On the other hand, the interfacial properties between alumina and samples A and B were determined by the previous sessile drop method under an oxygen partial pressure $5.4 \times 10^{-19}$ atm, respectively. Generally, the surface tension was calculated by the simplified Laplace Eq. [1] based on the profile parameters of molten steel.[10] It is known that the shape factor determines the surface tension; the density difference between molten steel and gas is a constant because the gas density is much smaller than that of liquid steel. Furthermore, the shape factor could be calculated by the empirical Eq. [2] proposed by Yildiz and Bashiry [24] Here, the shape factor is determined by the profile of

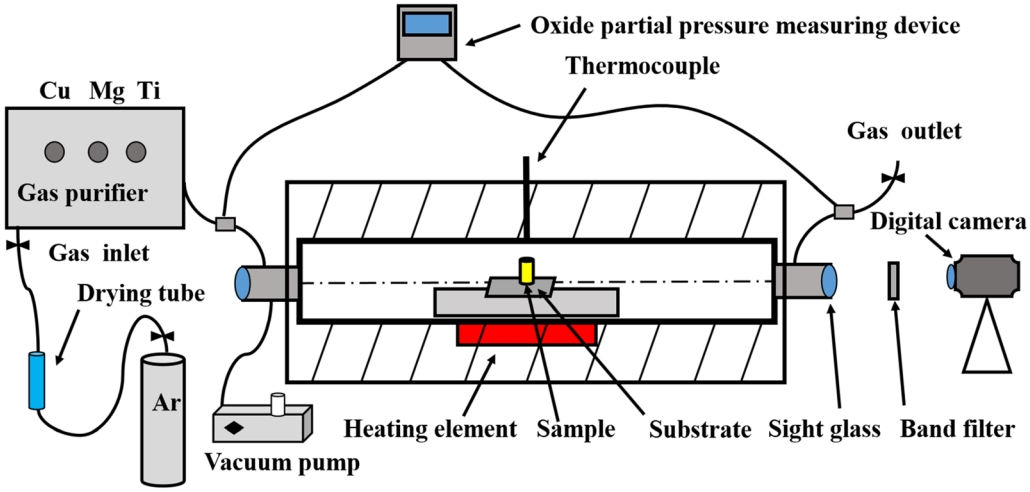


Fig. 4—Schematic diagram of the previous sessile drop method structure.

molten steel, including the x′ (m) and z′ (m), which present the farthest distance from the droplet vertex normal to the contour and the distance between the vertex and the line of two points on the furthest contour, respectively

$$\beta = \Delta\rho g R_0^2/\sigma_L \quad [1]$$

$$\beta = 46.327(2x'/z')^{(-3.735)} \quad [2]$$

where $\beta$ represents the shape factor of molten, $\Delta\rho$ represents the density difference between molten steel and gas phase (kg/m$^3$), $R_0$ represents the the curvature radius at apex point of droplet (m), and $\sigma_L$ represents the surface tension of molten steel (N/m).

### A. *Microscopic Interface Analysis*

After the termination of the experiments, the samples were taken out of the furnace, and the interface region between molten steel and the alumina substrate was analyzed microscopically in order to obtain information on the nature of the interaction and the possible formation of reaction products. The chemistry, morphology and microstructure of both sides (metal and substrate) of the interface were determined using a scanning electron microscope (SEM) with an energy dispersive X-ray spectroscopy (EDS) facility. There was an interface layer, and it was scraped off from the substrate, then the crystalline phase was analyzed using X-ray diffraction (XRD).

## IV. RESULTS

### A. *Wetting Behavior and Surface Tension of Interstitial-Free Molten Steel*

Figures 5 shows the melting droplet profile of interstitial-free molten steel for samples (a) A and (b) B with the previous used sessile drop method. It can be seen that the cylinder samples gradually melt into a hemispherical shape on the alumina substrate. Obviously, the contact angle between molten steel and an alumina substrate decreases with the titanium concentration. And, the vertex point arc radius of the semicircle increases with the titanium concentration, which indicates the wetability increases as titanium concentration increases.

Figures 6 and 7 show the melting droplet profile of molten steel for samples A and B, respectively, with the improved sessile drop method. When the molten steel contacted the alumina substrate before the recalescence occurred, the stable profile of the droplet and the contact angle between the alumina substrate and the molten steel were recorded. On the one hand, it is recorded that the dynamic wetting behavior between molten steel and an alumina substrate. At 0.2 seconds, the distance between the droplet apex and the substrate becomes the shortest, forming a maximum contact angle called the "advancing contact angle. At 0.6 seconds, the distance between the droplet apex and the substrate becomes the longest, forming a minimum contact angle called the receding contact angle. After 1.0 second, that forms a static contact angle. And, the difference between the advancing and receding contact angles for the molten steel with a titanium concentration of 540 ppm is lower than that with a titanium concentration of 280 ppm. On the other hand, the vertex point arc radius of the semicircle of molten steel and the contact area between molten steel and an alumina substrate appeared to increase with increasing titanium concentration, which was similar to the previous sessile drop method. However, the vertex point arc radius of the semicircle and the contact area between molten steel and alumina substrates are smaller than the results for the previous sessile drop method.

Therefore, the surface tension can be calculated by the shape parameters of interstitial-free molten steel with the two methods for samples A and B, as shown in Figure 8. It can be seen that the surface tension decreases with increasing titanium concentration for both the previous sessile drop method and the improved method. However, the results of the improved sessile drop method are greater

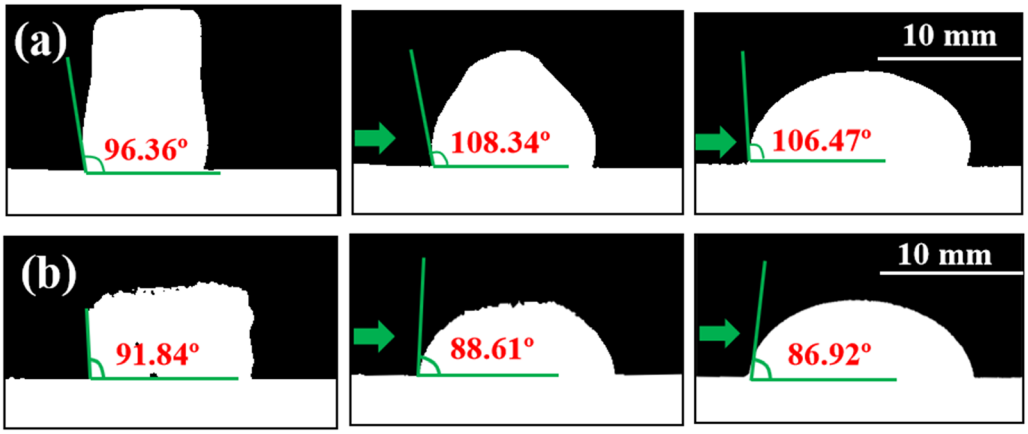


Fig. 5—Droplet profile of molten steel for samples (*a*) A and (*b*) B with the previous used sessile drop method.

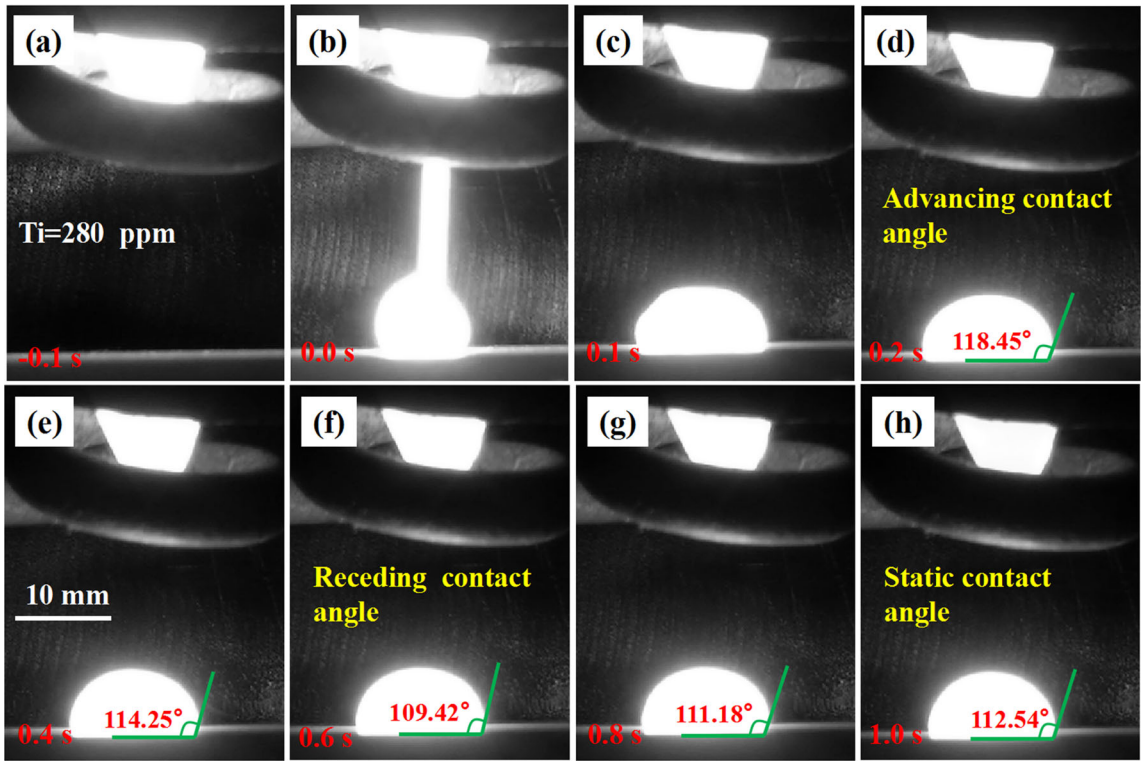


Fig. 6—Droplet profile of molten steel contacting alumina substrate for sample A with the improved sessile drop method at (*a*) -0.1 s, (*b*) 0.0 s, (*c*) 0.1 s, (*d*) 0.2 s, (*e*) 0.4 s, (*f*) 0.6 s, (*g*) 0.8 s, and (*h*) 1.0 s, respectively.

than those of the previous sessile drop method. Especially, the surface tension of molten steel is remarkably decreasing with increasing the active alloy element content with the previous sessile drop method. When the titanium concentration is 280 ppm, the difference in surface tension between the two methods is 55.481 mN/m, and when the titanium concentration is 540 ppm, the difference in surface tension between the two methods is 237.141 mN/m. Compared with the obtained surface tension and the work of other researchers, it was found that the present results from including the previous sessile drop method and the improved sessile drop method were slightly lower than those in Figure 8.[25–27] This could be because there are active elements such as O , S and P in the containing alloy steel that approach the actual steel composition.[28,29]

### B. *Contact Angle and Interfacial Tension Between Interstitial-Free Molten Steel and Alumina*

The static contact angle between the interstitial-free molten steel and the alumina can be measured by Image-J processing software when the droplet stabilizes on the alumina substrate. And, the interfacial tension

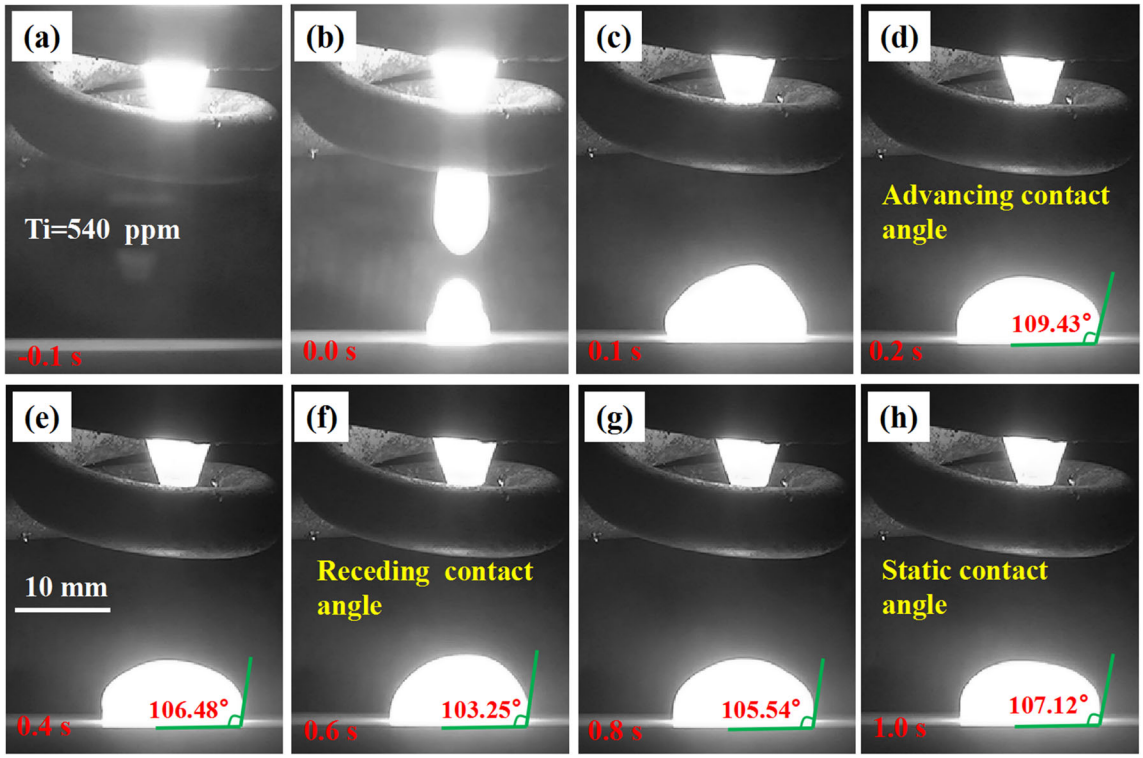


Fig. 7—Droplet profile of molten steel contacting alumina substrate for sample B with the improved sessile drop method at (*a*) -0.1 s, (*b*) 0.0 s, (*c*) 0.1 s, (*d*) 0.2 s, (*e*) 0.4 s, (*f*) 0.6 s, (*g*) 0.8 s, and (*h*) 1.0 s, respectively.

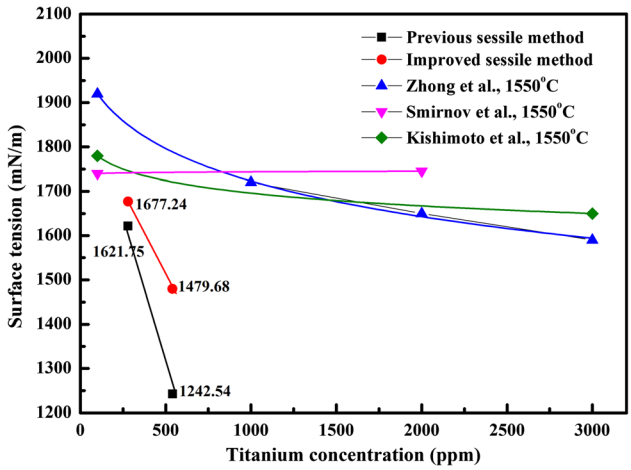


Fig. 8—Comparison surface tension for samples A and B for the previous sessile drop method and the improved sessile drop method with other researchers.

between interstitial-free molten steel and alumina can be calculated by Young' Eq. [3] based on the surface tension of molten steel and the contact angle.[10]

$$\sigma_{LP} = -\sigma_L cos\theta_{LP} + \sigma_P \quad [3]$$

where $\sigma_P$ is the surface tension of the alumina plate (N/m), $\sigma_{LP}$ is the interfacial tension of the molten steel (N/m), and $\theta_{LP}$ is the contact angle between molten steel and alumina (deg). The surface tension of alumina is given by Eq. [4].[30]

$$\sigma_P(\mathrm{mN/m}) = 2077 - 0.7083T \quad [4]$$

where T is the Kelvin temperature of the alumina plate, Therefore, the contact angle and the calculated interfacial tension for samples A and B between molten steel and alumina are plotted as shown in Figure 9. It can be seen that interfacial tension is 1428.71 mN/m and 1221.35 mN/m, respectively, with titanium concentrations of 280 ppm and 540 ppm for the improved sessile drop method, is higher than for the previous sessile drop method, which is 1245.56 mN/m and 719.01 mN/m, respectively. Similarly, the stable contact angle measured with the improved sessile drop method are higher than with the previous sessile drop method. On the other hand, the difference between the two methods is greater with increasing concentrations of the titanium alloy element.

This difference between the two methods may have two aspects. On the one hand, the molten steel contains other active alloying elements that wet, which leads to chemical reactions and solute segregation that are interactively coupled with the alumina substrate due to long-term contacting.[31] On the other hand, the liquid metal is not in direct contact with the initial nonreactive substrate, but with the new compound formed at the metal/ceramic interface due to the chemical reaction accompanying the wetting process in an incompletely purified atmosphere.[32,33]

Generally, the wetting in reactive systems is governed more by the final interfacial chemistry at the triple line than by the intensity of interfacial reactions.[34,35] This means that even a very thin reaction layer may

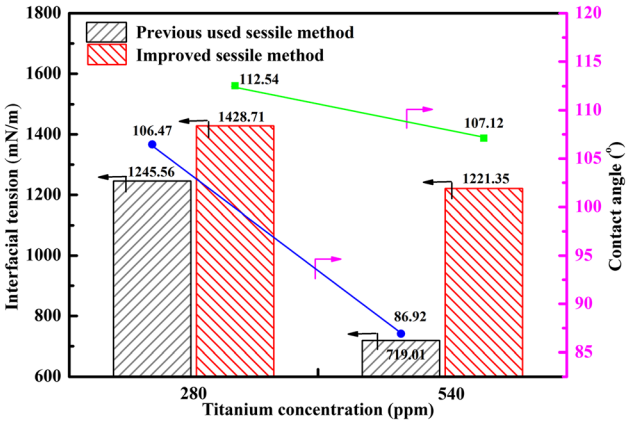


Fig. 9—Interfacial tension and contact angle between molten steel and alumina substrate for samples A and B with the previous sessile drop method and improved sessile drop method.

profoundly affect the wetting behavior.[36] It also has been reported that substantial additions of titanium are known to induce steel melts to wet alumina due to the formation of a Ti-rich reaction product at the alloy/ceramic interface, but the work has shown that even low Ti concentrations can induce a reactive wetting process leading to an improvement of the wettability of alumina by Fe alloys with the previous sessile drop method.[37]

However, the characteristics of the interface between interstitial-free molten steel and alumina aren't what the sessile drop method really wants to measure. Actually, the alloying of trace alloy titanium could react with an alumina substrate, which causes differences in the surface tension of molten steel, interfacial tension and contact angle between the molten steel and the inclusions due to the formed interface layer. It is lower than reality interface parameters between interstitial-free molten steel and alumina with the previous sessile drop method.

### C. *Microscopic Interface Layer Analysis*

In order to understand why the two methods have the same difference, the interface between steel and the alumina substrate with sample B after the sessile drop method under oxygen partial pressure $5.4 \times 10^{-23}$ atm was analyzed by SEM-EDS, as shown in Figure 10. Here, the steel sample was replaced by resin in the experiment in order to more conveniently observe the interface layer. It can be seen that an interface layer of about 3.5 $\mu$m could be produced between molten steel and an alumina substrate with a titanium concentration of 540 ppm for the previous sessile drop method in Figure 10(a), but not for the improved sessile drop method in Figure 10(b). And the interface layer is composed of an oxygen element and active metal elements, including Al, Si, Mn, Ti and Fe, which could be from the interstitial-free steel. As we know, it couldn't form the Fe-oxidization for melting Fe when the oxide partial pressure was less than $10^{-14}$ MPa. Therefore, it is easy to understand that the oxygen partial pressure and active metal elements in interstitial-free steel could play an important role in forming the interface layer, which needs further research to clarify the interface reaction mechanism. Obviously, the results with the improved sessile drop method are more reasonable due to the nonreactive interface characteristic between the interstitial-free molten steel and an alumina substrate. Furthermore, when the improved sessile drop method was used, the crack formation for an alumina substrate was found, as shown in Figure 10(b). This could be due to the small coefficient of thermal transfer exhibited by almost ceramic materials, which leads to thermal stresses during the spreading process.

Furthermore, the same process as above for the previous sessile drop method was performed with samples A and B under the oxygen partial pressure was $5.4 \times 10^{-19}$ atm. The interface layer after the previous sessile drop method was analyzed as shown in Figure 11. It can be seen that the thickness of the interface layer increase from 54.6 to 77.8 $\mu$m as titanium concentration increase from 280 to 540 ppm under the oxygen partial pressure $5.4 \times 10^{-19}$ atm. And the interface layer is composed of an enriching Al layer approaching an alumina substrate and an enriching Fe layer approaching molten steel as shown in Figure 11. Obviously, the reaction became more intense, and the interface layer became thicker with increasing titanium concentration and oxygen partial pressure.

Further, as we know, the Al, Mn, Si and Ti are the main deoxidizing elements during the refining process of molten steel.[38,39] It is due to these active metal intensive binding abilities with oxygen in molten steel that non-metallic inclusions are produced. In the metallurgical process, several deoxidizing elements could form composite inclusions.[40,41] Figure 12 shows the XRD of the interface layer with samples A and B after the previous sessile drop method under an oxygen partial pressure $5.4 \times 10^{-19}$ atm. As shown in Figure 12, it can be seen that the main phase is composed of composite oxides, including alumina, augite and magnetite with a titanium concentration of 280 ppm. The peak of iron aluminum titanium oxide appears as the content of the titanium alloying element increases, and the peak of alumina becomes weaker, which indicates that the reaction becomes more intense and complicated as the alloying element concentration increases.

## V. DISCUSSION

### A. *Analysis the Dynamic Contact Angle for Improved Sessile Drop Method*

Generally, when the force is balanced, the droplet woud form a static contact angle. However, the droplets on a plane with a certain angle ($\alpha$) could form advancing and receding contact angles ($\theta_a$ and $\theta_r$) respectively, due to the gravitational component force formed by the inclined plane. It can be seen that the advancing and receding contact angles are caused by the angle between the inclined plane and the horizontal plane in Figure 13(a), and the relationship between the total force and the difference of the advancing and receding contact angles can be expressed according to the Eq. [5].[42]

$$F = m\ g\ \sin\alpha = nd\ \sigma_L\ g\ (\cos\theta_r \cdot\ \cos\theta_a) \qquad [5]$$

where the F represents the total force (N), the m represents the weight of droplets (m), the $\alpha$ represents the angle between the inclined plane and the horizontal

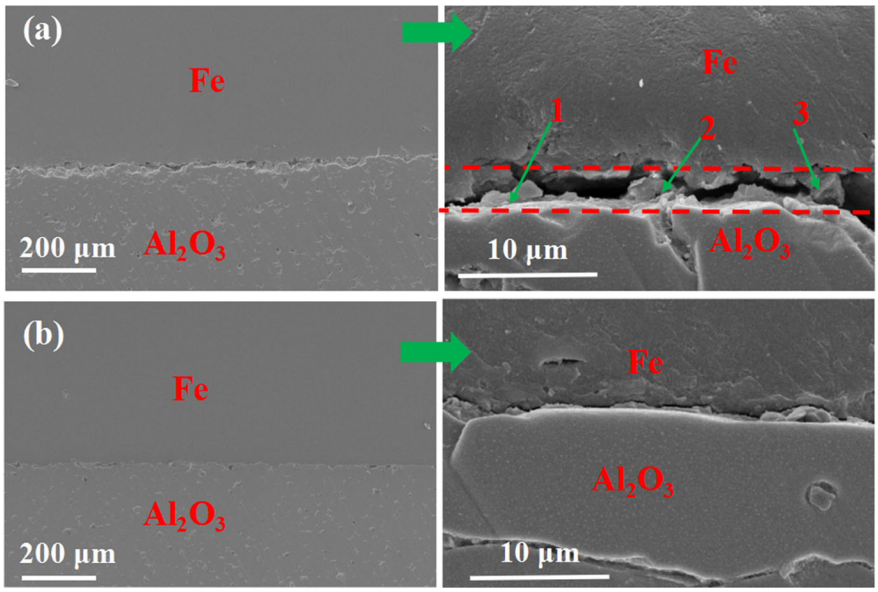


| 1# | |
|---|---|
| O | 35.13 |
| Al | 1.33 |
| Si | 1.75 |
| Mn | 1.41 |
| Fe | 60.38 |

| 2# | |
|---|---|
| C | 43.63 |
| O | 18.06 |
| Fe | 0.12 |
| Al | 14.86 |
| Ti | 1.14 |

| 3# | |
|---|---|
| C | 67.22 |
| O | 10.81 |
| Al | 1.13 |
| Si | 0.44 |
| Mn | 2.74 |

Fig. 10—SEM-EDS of the interface layer between molten steel and alumina substrate for sample B under oxygen partial pressure $5.4 \times 10^{-23}$ atm with (*a*) previous sessile drop method and (*b*) improved sessile drop method.

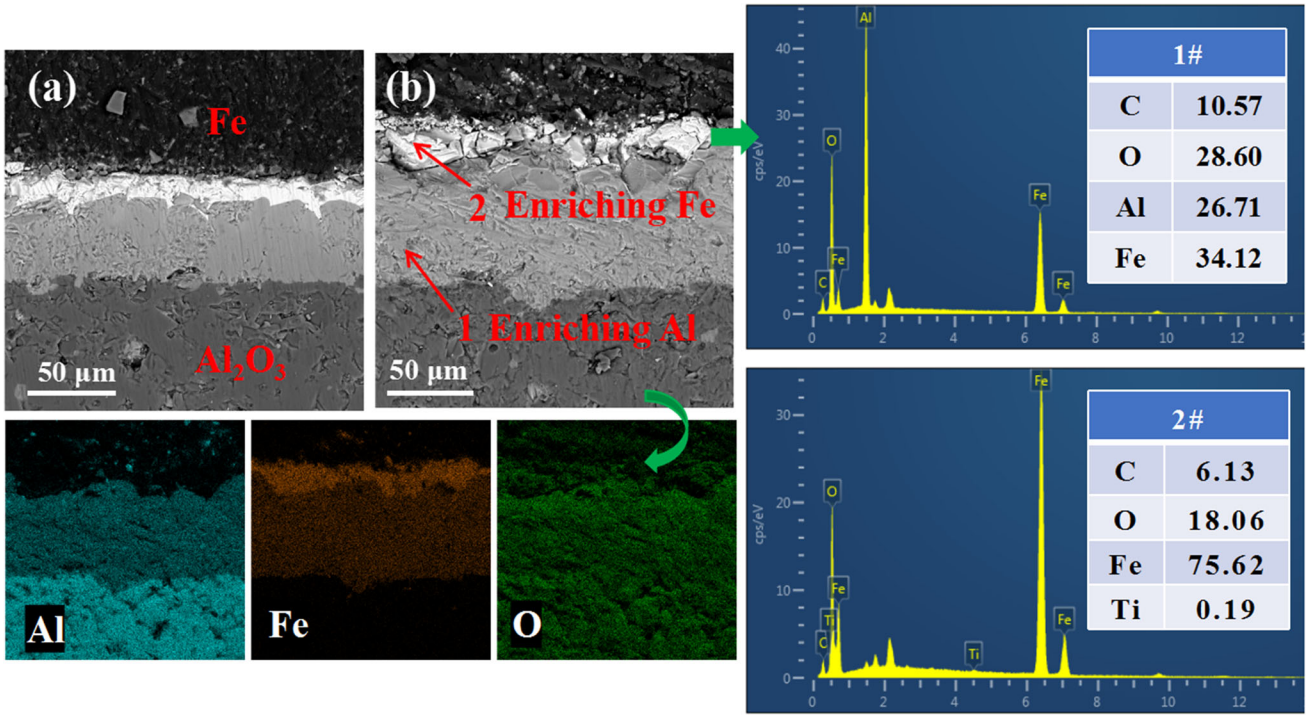


| 1# | |
|---|---|
| C | 10.57 |
| O | 28.60 |
| Al | 26.71 |
| Fe | 34.12 |

| 2# | |
|---|---|
| C | 6.13 |
| O | 18.06 |
| Fe | 75.62 |
| Ti | 0.19 |

Fig. 11—SEM-EDS of the interface layer between molten steel and alumina substrate with the previous sessile drop method under oxygen partial pressure $5.4 \times 10^{-19}$ atm for samples (*a*) A and (*b*) B.

plane (deg), the n represents the droplet profile correction parameter, the $\sigma_L$ represents the surface tension of molten steel, the g represents the acceleration of gravity ($m/s^2$); the $\theta_a$ and $\theta_r$ present respectively the advancing and receding angle (deg).

Similarly, the force analysis of the droplet dropped on the alumina substrate can be represented by Figures 13(b) through (d). Figure 13(b) represents the force analysis of the droplet and the alumina substrate at the advancing contact angle. The support force ($F_N$ is greater than the gravity (mg) at the interface between the substrate and the droplet owing to the impact force caused by the droplet falling. Due to the fluidity of the droplet and the rigidity of the substrate, the molten steel inside the droplet will be squeezed outward, forming a outward shear force ($F_S$) parallel to the substrate. Further, Figure 13(c) represents the force analysis of the droplet and the alumina substrate at the receding contact angle. The support force ($F_N$ is

smaller than the gravity (mg) at the interface between the substrate and the droplet, owing to the elasticity of the droplet going back. Due to the molten steel-argon interface barrier, the external molten steel is squeezed inward, forming an inward shear force ($F_S$) parallel to the substrate. Obviously, both the outward shear force and the inward shear force are similar with the total force of Figure 13(a).

It is proposed that the dynamic contact angles of droplets owing to fluidity reflect surface properties more accurately than values obtained from static and quasi-static measurements.[43] Although a large number of studies have reported that droplets fall on a flat surface, the function of contact angle as a function of droplet velocity, height, and mass has not been clearly defined.[44,45] Assuming that during the whole process, the droplet contacts the rigid alumina and reaches the lowest point for the droplet vertex, it performs a uniform deceleration motion with time $t_1$; 2) the two symmetrical shear forces ($F_S$) that are balanced on the substrate are the K times for the support force ($F_S = k\ F_N$) formed by the deceleration fluid molecule. The total force is the difference between the supporting force and the gravity as in Eq. [6], secondly, the total force can be obtained due to uniform deceleration with $t_1$ from the velocity obtained by the free-fall at height H as in Eq. [7]. Hence, the relationship between the height from the front of the quartz tube to the alumina substrate and the difference of advancing and receding contact angles can be simply expressed as Eq. [8].

$$F = F_N - mg \quad [6]$$

$$F = m\frac{\sqrt{2gH}}{t_1} \quad [7]$$

$$k\ m\left(\frac{\sqrt{2gH}}{t_1} + g\right) = nd\sigma_L\ g(\cos\theta_r \cdot \cos\theta_a) \quad [8]$$

where H presents the height between the front of the quartz tube and the alumina substrate (m), the $t_1$ present the time from the molten steel contacting the substrate to the highest point of the droplet profile descended to the lowest point (s). It can be seen that the greater the height, the greater the dynamic contact angle, which is consistent with the reported low Reynolds numbers due to height for water droplets.[46,47] And, it can also be seen that the difference in contact angle between advance and receding can be changed by adjusting the height and mass of the droplet.

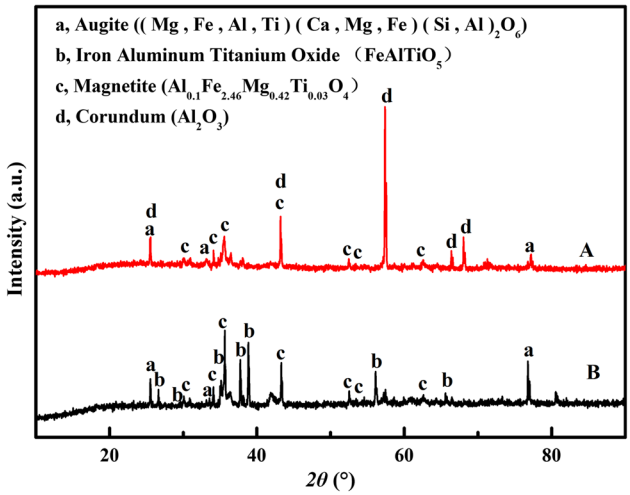


Fig. 12—XRD of the interface layer after the previous sessile drop method under oxygen partial pressure $5.4 \times 10^{-19}$ atm for samples A and B.

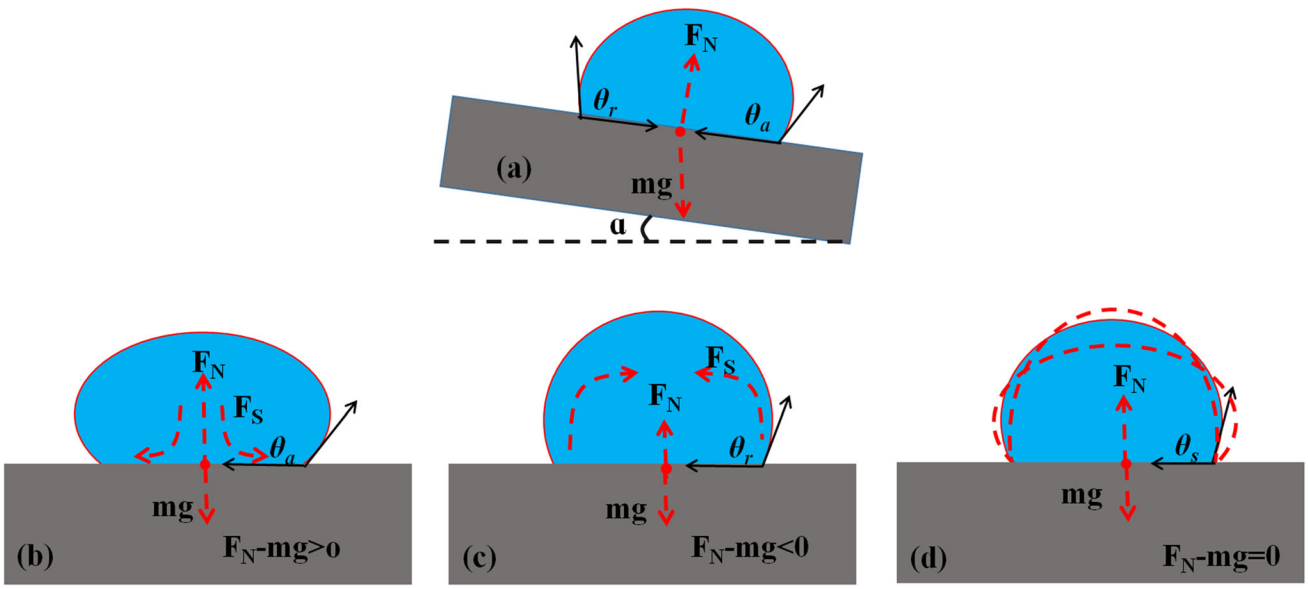


Fig. 13—Forces analysis for (*a*) droplets on a plane with a angle of α and dynamic droplet on the alumina substrate when (*b*) $F_N$ is greater than the gravity, (*c*) $F_N$ is smaller than the gravity, and (*d*) $F_N$ is equivalent to the gravity.

As shown in Figures 13(b) and (c), the advancing and receding contact angles can more realistically reflect the wetting behavior between the flowing molten steel and solid material because the liquid steel is always flowing in the actual steel-making process. And Figure 13(d) shows that the support force ($F_N$) is equivalent to the gravity (mg) at the interface between the substrate and the droplet, and the formed static contact angle ($\theta$s) is similar to the contact angle of the sessile drop method. Consequently, the static molten steel profile and the contact angle can be used as parameters for the calculated surface tension of molten steel and the interfacial tension between the molten steel and the alumina ceramic matrix. This improved sessile drop method can simultaneously obtain both dynamic and static contact angles.

### B. *Interface Reaction Between Low Alloy Molten Steel and Alumina*

The observed reactive-wetting behavior for alloy containing molten steel was a consequence of the formation at the Fe-Ti/$Al_2O_3$ interface of an oxide layer. For the oxygen contents expected in the Fe drop, the stable interface phase would be hercynite ($FeAl_2O_4$), which was formed according to the Eq. [9].[37]

$$Fe + [O] + Al_2O_3 = FeAl_2O_4 \qquad [9]$$

As we know, in the metallurgical refining alloying process, the addition of titanium to a Fe melt results in reactions involving the dissolution of $Al_2O_3$ according to the following general Eq. [10].[48,49] Generally, the containing alloy elements in molten steel, including Al, Mn, Si, Ti and other elements, could also react with an alumina substrate under a particularly low oxygen partial pressure due to the stronger deoxidization capacity. From thermodynamics, Doo *et al.*[50] concluded that Ti exists in the form of a binary TiOx-$Al_2O_3$ phase in the inclusions observed in Ti-bearing Al-killed low carbon steels. The TiOx–$Al_2O_3$ inclusions were reported to be wetted more easily by the liquid Fe compared to the pure $Al_2O_3$ inclusions.[51] In the case of TiOx (*i.e.,* Ti oxides of varying oxidation states), reported values of the contact angle for $TiO_2$ with liquid Fe vary between 84 and 80°.[34,52] As a result of these low contact angle $\theta_{LP}$ values, the interfacial tension and contact angle between molten steel containing titanium alloy and alumina rapidly decline with the previous used sessile drop method.

$$[Ti] + \frac{x}{3}Al_2O_3 \rightarrow \frac{2x}{3}[Al] + TiO_x \qquad [10]$$

## VI. CONCLUSIONS

A new method was used to measure the dynamic wetting properties between high-temperature low alloy molten steel and a solid alumina substrate at 1550 °C. The unique conclusions can be obtained by comparing the previous sessile drop method with the following:

(1) The new method measured the dynamic wetting behavior, including the advance, receding and static contact angles between high-temperature low alloys molten steel and a solid alumina substrate. It can reflect the more realistic wetting behavior between high-temperature flow liquid and a solid substrate. And the difference in contact angle between advance and receding can be changed by adjusting the height between the front of the quartz tube and the alumina substrate. For the low alloy steel industry, it has a very wide range of application prospects in the fields of inclusion control, high-temperature refractory protection, high alloy steel mold casting and the solidification behavior of steel liquid in mold.
(2) The improved sessile drop method is more favorable for measuring the surface tension of interstitial-free molten steel and the interfacial tension between molten steel and an alumina substrate. It has been reduced for surface tension and interfacial tension due to the interaction between the contained alloy elements in molten steel and the alumina substrate producing an interface reaction involving active alloy elements such as Mn, Si and Ti. And, the extent of reaction relating to interface layer thickness increases with increasing the concentration of active alloy elements and the oxygen partial pressure of the protective atmosphere.


## ACKNOWLEDGMENTS

The financial support from the National Key Research and Development Program of China (No. 2021YFB3702401), the Hunan Scientific Technology Projects (No. 2020WK2003), and the National Science Foundation of China (No. 52130408) are greatly acknowledged.


## CONFLICT OF INTEREST

The authors declare that they have no known competing financial interests or personal relationships that could have appeared to influence the work reported in this paper.

## REFERENCES


1. D.X. Yin, M.A. Pei-Sheng, and S.Q. Xia: *Bull. Sci. Technol.*, 2007, vol. 23, pp. 424–29.
2. A.A. Amadeh, J.C. Labbe, and P.E. Quintard: *J. Eur. Ceram. Soc.*, 2005, vol. 25, pp. 1041–48.
3. H. Ohba and K. Sugita: *J. Ceram. Soc. Jpn.*, 1963, vol. 71, pp. 207–13.
4. J. Kurikkala, O. Mattila, T. Fabritius, and J. Härkki: *ISIJ Int.*, 2010, vol. 50, pp. 356–62.
5. Q. Shu, T. Alatarvas, V. Visuri, and T. Fabritius: *Metall. Mater. Trans. B*, 2021, vol. 52B, pp. 1818–29.
6. K. Sasai: *ISIJ Int.*, 2016, vol. 56, pp. 1013–22.
7. C. Lu, W. Wang, J. Zeng, C. Zhu, and J. Chang: *Metall. Mater. Trans. B*, 2019, vol. 50B, pp. 77–85.

8. J.M. Ludwicki, F.L. Robinson, and P.H. Steen: *ACS Appl. Mater. Interfaces*, 2020, vol. 12, pp. 22115–19.
9. P.S. Marquis de Laplace: *Traité de Mécanique Céleste*, Courcier, Paris, 1805.
10. T. Young: *Philos. Trans. R. Soc. Lond.*, 1805, vol. 95, pp. 65–87.
11. H. Daikoku, S. Kawanishi, T. Ishikawa, and T. Yoshikawa: *J. Chem. Thermodyn.*, 2021, vol. 160, p. 106476.
12. J.P. Anson, R. Drew, and J.E. Gruzleski: *Metall. Mater. Trans. B*, 1999, vol. 30B, pp. 1027–32.
13. M.G. Cabezas, A. Bateni, J.M. Montanero, and A.W. Neumann: *Langmuir*, 2006, vol. 22, pp. 10053–60.
14. B. Gallois and C. Lupis: *Metall. Mater. Trans. B*, 1981, vol. 12B, pp. 549–57.
15. J. Lee, T. Tanaka, M. Yamamoto, and S. Hara: *Mater. Trans.*, 2005, vol. 45, pp. 625–29.
16. J. Schmitz, J. Brillo, I. Egry, and R. Schmid-Fetzer: *Int. J. Mater. Res.*, 2013, vol. 100, pp. 1529–35.
17. Tolman; and C. Richard: J. Chem. Phys., 1949, vol. 17, pp. 333–37.
18. S.C. Hardy: *J. Cryst. Growth*, 1984, vol. 69, pp. 456–60.
19. S. Ozawa, S. Takahashi, S. Suzuki, H. Sugawara, and H. Fukuyama: *Jap. J. Appl. Phys.*, 2011, vol. 50, p. 11.
20. S. Ozawa, S. Takahashi, N. Watanabe, and H. Fukuyama: *Int. J. Thermophys.*, 2014, vol. 35, pp. 1705–11.
21. Q. Li, H. Zhang, M. Gao, J. Li, and H. Zhang: *J. Mater. Process. Tech.*, 2021, vol. 294, p. 117094.
22. L. Liu, T.H. Wang, J.C. Li, and Q. Jiang: *Solid State Commmun.*, 2012, vol. 15, pp. 573–76.
23. X.U. Qian-Gang, Z. Hai-Feng, and H.U. Zhuang-Qi: *Trans. Nonferr. Metal. Soc.*, 2005, vol. 15, pp. 45–50.
24. B. Yildiz and V. Bashiry: *J. Adhes.*, 2018, vol. 95, pp. 929–42.
25. M. Kishimoto, K. Mori, and Y. Kawai: *ISIJ Int.*, 1984, vol. 48, pp. 413–17.
26. L.C. Zhong, M. Zeze, and K. Mukai: *Acta Metall. Sin.*, 2004, vol. 17, pp. 795–804.
27. M. Divakar, J.P. Hajra, A. Jakobsson, and S. Seetharaman: *Metall. Mater. Trans. B*, 2000, vol. 31, pp. 267–76.
28. K. Ogino, K. Nogi, and C. Hosoi: *Tetsu- to- Hagane*, 1983, vol. 69, pp. 1989–94.
29. T. Yokoyama, Y. Ueshima, K. Sasai, Y. Mizukami, H. Kakimi, and M. Kato: *Tetsu- to- Hagane*, 1997, vol. 83, pp. 563–68.
30. J. Lee, Y. Kim, J. Choe, and M. Abbasi: AISTech 2013, 2013, vol. 1, pp. 1117–22.
31. N. Eustathopoulos: *Acta Mater.*, 1998, vol. 46, pp. 2319–27.
32. K.C. Mills, E.D. Hondros, and Z. Li: *J. Mater. Sci.*, 2005, vol. 40, pp. 2403–409.
33. C. Wan, P. Kritsalis, B. Drevet, and N. Eustathopoulos: *Mater. Sc. Eng. A*, 1996, vol. 207, pp. 181–87.
34. P. Kritsalis, B. Drevet, N. Valignat, and N. Eustathopoulos: *Scr. Metall. Mater.*, 1994, vol. 30, pp. 1127–32.
35. K. Landry, C. Rado, and N. Eustathopoulos: *Metall. Mater. Trans. A*, 1996, vol. 27A, pp. 3181–86.
36. K. Landry, C. Rado, and R. Voitovich: *Acta Mater.*, 1997, vol. 45, pp. 3079–85.
37. A. Karasangabo and C. Bernhard: *J. Adhes. Sci. Technol.*, 2012, vol. 26, pp. 1141–56.
38. X. Cai, Y. Bao, L. Lin, and C. Gu: *Steel Res. Int.*, 2015, vol. 87, pp. 1168–78.
39. C.H. Chang, I.H. Jung, S.C. Park, H.S. Kim, and H.G. Lee: *Ironmak. Steelmak.*, 2013, vol. 32, pp. 251–57.
40. C. Wang, N. Verma, Y. Kwon, W. Tiekink, N. Kikuvhi, and S. Sridhar: *ISIJ Int.*, 2011, vol. 51, pp. 375–81.
41. C. Xuan, W. Mu, Z.I. Olano, P.G. Jnsson, and K. Nakajima: *Steel Res. Int.*, 2016, vol. 87, pp. 911–20.
42. C.G.L. Furmidge: *J. Colloid Interface Sc.*, 1962, vol. 17, pp. 309–24.
43. M. Remer, M. Psarski, K. Gumowski, J. Rokicki, G. Sobieraj, M. Kaliush, D. Pawlak, and G. Celichowski: *Colloids Surf. A*, 2016, vol. 508, pp. 57–69.
44. S. Sikalo, H.D. Wilhelm, I.V. Roisman, S. Jakirli, and C. Tropea: *Phys. Fluids*, 2005, vol. 17, pp. 62103.
45. S.F. Lunkad, V.V. Buwa, and K. Nigam: *Chem. Eng. Sci.*, 2007, vol. 62, pp. 7214–24.
46. J. Fukai, Z. Zhao, D. Poulikakos, C.M. Megaridis, and O. Miyatake: *Phys. Fluids A*, 1993, vol. 5, pp. 2588–99.
47. D. Roux and J.J. Cooper-White: *J. Colloid Interf. Sci.*, 2004, vol. 277, pp. 424–36.
48. B. Deo, and R. Boom: Prentice Hall International, London, UK, 1993.
49. W.Y. Kim, J.O. Jong-Oh, C.O. Lee, D.S. Kim, and J.J. Pak: *ISIJ Int.*, 2008, vol. 48, pp. 17–22.
50. W.C. Doo, D.Y. Kim, and K. Yi: *Met. Mater. Int.*, 2007, vol. 13, pp. 249–55.
51. S. Basu, S.K. Choudhary, and N.U. Girase: *ISIJ Int.*, 2004, vol. 44, pp. 1653–660.
52. M. Kudoh, K. Ohsasa, K. Tanaka, and K. Okuyama: Bull. Faculty Eng. Hokkaido University, 1992, vol. 162, pp. 191–202.